Available online at www.sciencedirect.com
SCIENCE DIRECT
Catalysis Today 107–108 (2005) 595–601
CATALYSIS TODAY
www.elsevier.com/locate/cattod

# Influence of thermal treatment on the structure and photocatalytic activity of $TiO_2$ P25

Nádia R.C. Fernandes Machado *, Veronice S. Santana

*Departamento de Engenharia Química, Universidade Estadual de Maringá, Av. Colombo 5790, Bloco D-90, CEP 87020-900, Maringá, Paraná, Brazil*

Available online 19 August 2005

**Abstract**

More stringent regulations concerning effluent release into rivers and streams have made it necessary to develop new technologies for effluent mineralization, with heterogeneous photocatalysis as an attractive option. The aim of the present work was to investigate the influence of thermal treatment on the structure and photocatalytic activity of $TiO_2$ P25. The $TiO_2$ was calcined at different temperatures (0, 200, 300, 400, 500, 600 and 700 °C) and used for phenol degradation (50 mg $l^{-1}$) under visible and near-UV irradiation for 5 h. Characterization analyses (textural analysis, acidity and X-ray diffraction (XRD)) showed that the specific surface area decreased with increasing calcination temperature from 500 to 700 °C, while the catalyst acidity increased after thermal treatment. The anatase–rutile phase transformation occurred at 600 °C. In this process, both direct and sensitized photocatalysis occurred and uncalcined $TiO_2$ showed the highest level of phenol degradation. An increase in calcination temperature led to a reduction in $TiO_2$ activity, which may be related to the presence of rutile and anatase phases, as well as to surface adsorbed water and hydroxyl groups on the $TiO_2$.


*Keywords:* $TiO_2$; Thermal treatment; Phenol; Photocatalysis

## 1. Introduction

Industries generally generate highly polluting effluents. Many of the pollutant properties of these effluents are attributed to phenolic compounds, mainly in the effluents of alcohol distilleries, due to their toxicity and capacity to inhibit conventional biological treatments [1].

As a consequence of this situation and more stringent regulations concerning effluent release into rivers and streams, new technologies have been developed to reduce these refractory contaminants. Among them, heterogeneous photocatalysis, an advanced oxidative process (AOP), has proved suitable for the ready elimination of phenolic compounds [2,3].

Recently, much attention has been paid to $TiO_2$ particles for environmental remediation by photocatalytic decomposition of waste materials and pollutants, due both to its high photoactivity in the degradation of organic compounds and its chemical/photocorrosion stability under various reaction conditions [4–7]. The bandgap energy of $TiO_2$ is 3.0–3.2 eV, which can be excited by UV light of wavelengths shorter than 385 nm. Thus, when $TiO_2$ absorbs a photon and is then promoted to an excited state, an electron is transferred from the valence band to the conduction band, where it can function as a reducing moiety, leaving a hole in the valence band that is a strong oxidizing moiety [8].

Many studies have been reported on the relations between crystallographic structure and surface properties and the effect of these properties on the photocatalytic properties [5,9–11]. Thus, the objective of this work was to investigate the influence of calcination temperature on the $TiO_2$ P25 structure and photocatalytic activity for phenol degradation.

## 2. Experimental

Degussa $TiO_2$ P25, used as a photocatalyst, was submitted to an agglomeration process (particle size range

* Corresponding author. Tel.: +55 44 32614747; fax: +55 44 32632652.
*E-mail address:* nadia@deq.uem.br (N.R.C. Fernandes Machado).

0920-5861/$ – see front matter © 2005 Elsevier B.V. All rights reserved.
doi:10.1016/j.cattod.2005.07.022

0.210–0.297 mm) and thermal treatment for 4 h at different temperatures (0, 200, 300, 400, 500, 600 and 700 °C).

### 2.1. Characterization

Textural analysis of the catalysts was carried out using $N_2$ gas adsorption–desorption isotherms at 77 K using Quantachrome Nova 1200 equipment. Surface area measurements were made according to the BET method and the pore size distribution was calculated using the *t*-method (micropores) and BJH method (mesopores) with data determined from the desorption branch of the isotherms.

A model reaction of isopropanol decomposition was used to characterize the acidic and basic properties of the catalysts, for which 0.1 g of catalyst was placed in a tubular reactor and submitted to activation in situ under a flow of $N_2$/He (30 ml $min^{-1}$) at a heating rate of 10 °C $min^{-1}$ and isothermal steps of 10 min at 100, 200 and 300 °C, and 90 min at 400 °C. The reaction was processed at 350 °C with isopropanol flow of 12.62 $cm^3$ $h^{-1}$. After condensation, liquid samples were collected at regular intervals of 20 min for 60 min. Analyses of the liquid products were carried out on a Varian 3300 gas chromatograph equipped with a thermal conductivity detector. The column used for analysis was 10% Carbowax 20M/Chromosorb W-HP with dimensions of 30 m × 1/8 in. It was not possible to characterize the uncalcined $TiO_2$ or $TiO_2$ calcined below 400 °C with this method, because the thermal treatment temperature was lower than the reaction temperature.

The zero point charge ($pH_{(ZPC)}$) of each catalyst was determined by agitating a suspension (1 g of catalyst and 30 ml of deionized water) for 24 h and then measuring the pH.

X-ray diffraction (XRD) measurements were carried out on a Ray-X Rigaku Miniflex diffractometer using Cu Kα irradiation, tension of 30 kV, current of 10 mA, a scanning speed of 2° $min^{-1}$, and intensity of 2000 cps.

### 2.2. Photocatalytic activity

Degradation tests were carried out in a refrigerated (33 °C), aerated (air flow 130 ml $min^{-1}$) and magnetically agitated reactor.

A 1 g sample of catalyst was suspended in 1 l of aqueous phenol solution (50 mg $l^{-1}$) at an initial pH of ∼8. The mixture was irradiated for 5 h with a 250 W high-pressure Hg lamp, emitting visible and near-UV light, located 15 cm above the solution surface. At regular intervals of 1 h, aliquots of 10 ml were collected, filtered through a Millipore filter (pore size 0.45 μm) and analyzed in TRACE GC ThermoFinnigan gas chromatograph equipped with a flame ionization detector (FID), using an OV Carbowax 20M (0.5 μm) fused silica capillary column with dimensions of 30 m × 0.25 mm. *o*-Cresol was used as the internal standard.

## 3. Results and discussion

### 3.1. Characterization of photocatalysts

Fig. 1 displays the nitrogen adsorption–desorption isotherms of the catalysts. It can be observed that uncalcined $TiO_2$ and $TiO_2$ thermally treated at 200 °C exhibited type II nitrogen isotherms. This type of isotherm is indicative of non-porous or macroporous material. These results are similar to those obtained by Saadoun et al. [9], who reported that Degussa $TiO_2$ P25 is a non-porous powder mixture of anatase and rutile phases, which showed the presence of mesopores after thermal treatment at 260 °C under vacuum for 24 h, as denoted by the hysteresis loop in its adsorption–desorption isotherm.

All other samples of $TiO_2$ calcined above 200 °C exhibited a type IV nitrogen isotherm with type H3 desorption hysteresis loops, indicative of their mesoporosity. As the number of mesopores decreased on thermal treatment above 500 °C, it is worth noting that the hysteresis loops exhibited for $TiO_2$ (600) and $TiO_2$ (700) – where the value in parentheses indicates the calcination temperature – are smaller than those observed for $TiO_2$ (300) and $TiO_2$ (400). In terms of adsorbed volume, $TiO_2$ (400) showed greater adsorption and hysteresis, indicative of a more porous material.

The hysteresis phenomenon in isotherms for physical adsorption is related to capillary condensation in mesoporous structures, in which the adsorbed volume tends to a finite maximum value, corresponding to complete filling of the capillary [12].

Table 1 shows the textural properties of the $TiO_2$ samples. It can be observed that the specific surface area (BET) remained practically constant for all samples, at nearly 42 $m^2$ $g^{-1}$, except for $TiO_2$ (600) and $TiO_2$ (700), for which the surface area decreased considerably as the calcination temperature increased, due to the particle agglomeration process.

The external surface area, total pore volume and mean pore diameter decreased as the temperature was increased from 300 to 700 °C.

The external surface area was estimated from the slope of a straight line fitted for the linear part of the *t*-plot. The intercept of the straight part on the axis for the adsorbed amount represents the micropore volume [13]. As the choice of fitting range is an open subject, we chose the interval 0.6–0.7 $P/P_0$, which led to the best straight line for the samples.

It has been established that the surface area, porosity, and pore volume decrease several-fold after heat treatment in the temperature range 450–900 °C, whereas the pore diameter increases. The main reason for this change in pore structure in this temperature range is attributed to sintering and/or phase transformations occurring in these materials [14].

$TiO_2$ is a material with characteristic mesoporosity after thermal treatment. The mean pore diameter considerably

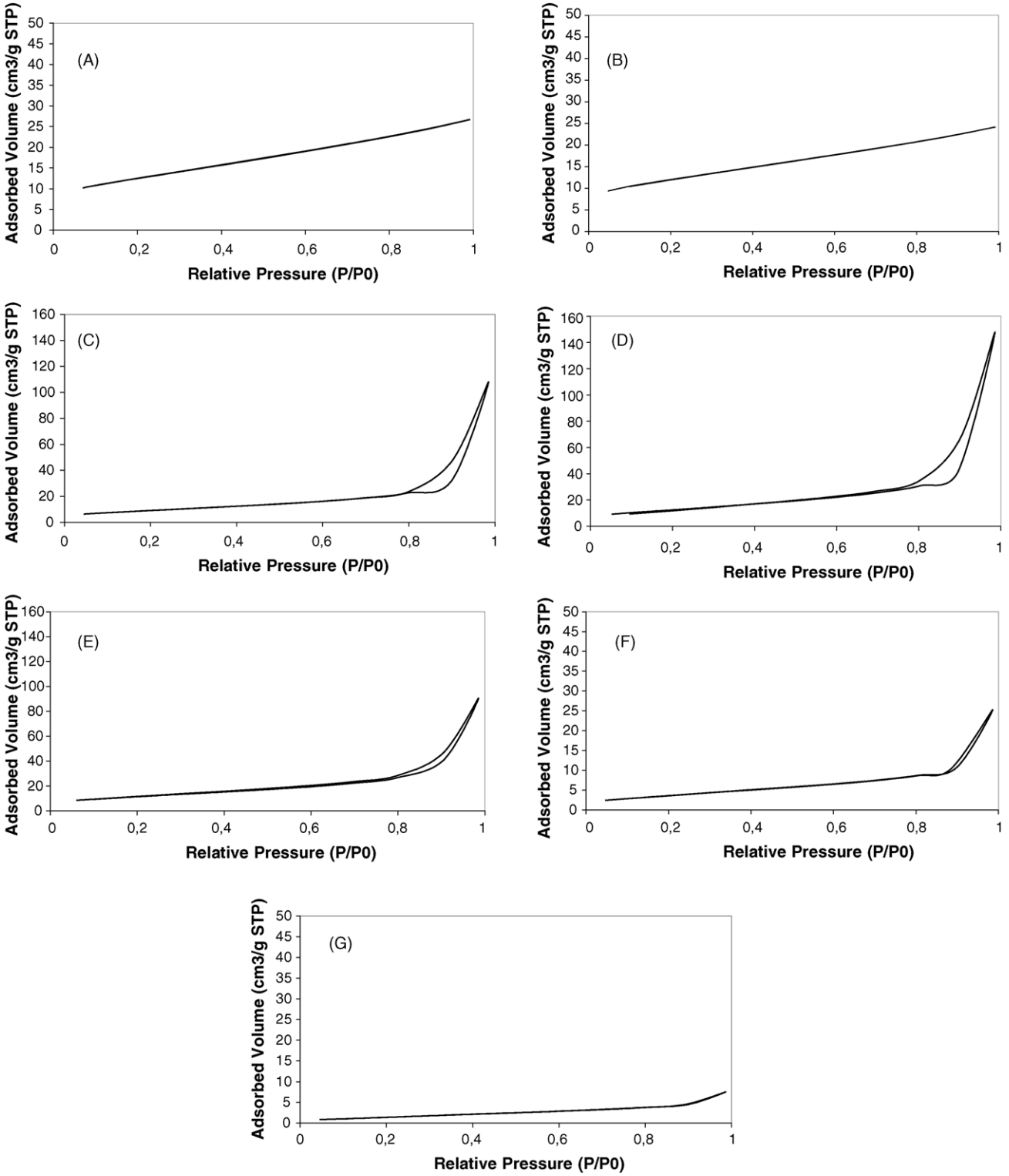


Fig. 1. $N_2$ adsorption–desorption isotherms for: (A) $TiO_2$ (uncalcined); (B) $TiO_2$ (200); (C) $TiO_2$ (300); (D) $TiO_2$ (400); (E) $TiO_2$ (500); (F) $TiO_2$ (600); (G) $TiO_2$ (700).

decreased after thermal treatment; it changed from 198 Å (300 °C) to 82 Å (700 °C).

The $TiO_2$ surface acidity was also studied to gain greater understanding of the physical nature of these photocatalysts.

From a mechanistic point of view, alcohol decomposition on solid catalysts occurs as follows: (1) dehydration is generally catalyzed by acidic sites, and (2) dehydrogenation is catalyzed by basic sites, or both acidic and basic sites.

Table 1
Textural analysis of $TiO_2$ thermally treated

| Catalyst | Specific surface area ($m^2/g$)[a] | External surface area ($m^2/g$)[b] | Micropores area ($m^2/g$)[c] | Mesopores area ($m^2/g$)[d] |
|---|---|---|---|---|
| $TiO_2$ (uncalcined) | 44 | 44 | 0 | 0 |
| $TiO_2$ (200) | 42 | 42 | 0 | 0 |
| $TiO_2$ (300) | 34 | 34 | 0 | 32 |
| $TiO_2$ (400) | 46 | 45 | 1 | 33 |
| $TiO_2$ (500) | 42 | 39 | 3 | 24 |
| $TiO_2$ (600) | 14 | 12 | 2 | 6 |
| $TiO_2$ (700) | 6 | 5 | 1 | 3 |

[a] Calculated by BET method.
[b] Calculated by *t*-method employing de Boer pattern isotherm.
[c] Calculated by *t*-method employing de Boer pattern isotherm.
[d] Calculated by BJH method (desorption branch).

Thus, isopropanol decomposition was used to characterize the acidic and basic properties of the catalysts. The acidity is related to the rate of dehydration (propene formation), while the basicity is related to the ratio of dehydrogenation (acetone formation) to dehydration [10,15].

The surface of $TiO_2$ has both acidic and basic sites. The acidic sites are associated with coordinately unsaturated surface metal ions, while the basic sites are associated with surface anions or anion vacancies [15].

Thermal treatment influenced the acidity; however, this influence did not follow the same trend as reported in the literature, where an increase in calcination temperature caused a reduction in acidity [10]. The results in Table 2 show the opposite of this behavior: the catalyst acidity increased with increasing calcination temperature. This increase was more significant in $TiO_2$ (600) and $TiO_2$ (700) and it can be attributed to polymorphic transformation, since $TiO_2$ (500) shows mixed crystallite phases and $TiO_2$ (700) presents only the rutile phase.

In terms of acidity during the reaction, catalysts thermally treated at 400 and 600 °C showed random results, while $TiO_2$ (500) and $TiO_2$ (700) showed a reduction in acidity, mainly at the end.

Evaluation of the catalyst characteristics during the reaction showed an increase in basicity, mainly for $TiO_2$ (600) and $TiO_2$ (700). The same behavior could be verified in terms of the increase in calcination temperature. However, for $TiO_2$ (500) the behavior was different. It did not produce acetone during the first 20 min, after which production reached a constant value until the end of the reaction.

Thermal treatment led to a reduction in isopropanol total conversion, although this reduction was not very significant. During the reaction, it was verified that the catalysts suffered deactivation of nearly 15%, except for $TiO_2$ (700), with deactivation of 24%.

At pH values above the $pH_{(ZPC)}$, the surface of the catalyst is negatively charged and, conversely, below the $pH_{(ZPC)}$ it is positively charged [16].

According to the literature [15,17], $pH_{(ZPC)}$ values are strongly affected by high-temperature pretreatment of the oxide. Titania has amphoteric character and the $pH_{(ZPC)}$ of $TiO_2$ P25 is 6.8. We observed that $TiO_2$ without thermal treatment, $TiO_2$ (200) and $TiO_2$ (300) showed acid characteristics and the $pH_{(ZPC)}$ values increased with increasing calcination temperature. $TiO_2$ (700) had a slightly basic pH value. Table 3 presents a summary of the $pH_{(ZPC)}$ values of the catalysts.

These results are opposed to the acidity results obtained for the model reaction and those of Pelizzetti and Minero [17], who reported that calcination of $TiO_2$ samples above 800 °C resulted in a decrease in $pH_{(ZPC)}$. Such a decrease in the $pH_{(ZPC)}$ values was attributed to irreversible changes in the surface chemistry of $TiO_2$ [17].

The fraction of rutile and anatase crystalline phases present in each sample and the temperature of the anatase–rutile phase transformation were identified by XRD and on the basis of the JCPDS data bank.

Fig. 2 shows XRD patterns for the samples. The intensities of the anatase peaks decreased, while the intensities of the rutile peaks greatly increased as the calcination temperature was raised.

Table 2
Model reaction of the isopropanol decomposition

| Catalyst[a] | Specific acidity (mmol propene/(h $m^2$)) | | | Specific basicity (μmol acetone/(h $m^2$)) | | | Acetone formation/propene formation [$r_A/r_P$] (E-3) | | | Total conversion (%) | | |
|---|---|---|---|---|---|---|---|---|---|---|---|---|
| | 20′ | 40′ | 60′ | 20′ | 40′ | 60′ | 20′ | 40′ | 60′ | 20′ | 40′ | 60′ |
| $TiO_2$ (400) | 9 | 8 | 8 | 32 | 66 | 78 | 7 | 8 | 9 | 55 | 53 | 45 |
| $TiO_2$ (500) | 9 | 8 | 8 | 0 | 100 | 90 | 0 | 12 | 11 | 50 | 44 | 43 |
| $TiO_2$ (600) | 16 | 21 | 16 | 156 | 243 | 320 | 10 | 11 | 20 | 41 | 39 | 35 |
| $TiO_2$ (700) | 41 | 37 | 33 | 513 | 970 | 1070 | 12 | 26 | 32 | 42 | 35 | 32 |

[a] Values in parenthesis show calcination temperature in °C.

Table 3
Zero point charge ($pH_{(ZPC)}$) of $TiO_2$ samples

| Catalyst | $pH_{(ZPC)}$ |
|---|---|
| $TiO_2$ (uncalcined) | 3.52 |
| $TiO_2$ (200) | 3.61 |
| $TiO_2$ (300) | 3.77 |
| $TiO_2$ (400) | 5.45 |
| $TiO_2$ (500) | 6.41 |
| $TiO_2$ (600) | 6.61 |
| $TiO_2$ (700) | 7.41 |

Table 4
Anatase and rutile crystalline phases of $TiO_2$

| Catalyst | Anatase fraction (%) | Rutile fraction (%) |
|---|---|---|
| $TiO_2$ (uncalcined) | 83 | 17 |
| $TiO_2$ (200) | 82 | 18 |
| $TiO_2$ (300) | 82 | 18 |
| $TiO_2$ (400) | 82 | 18 |
| $TiO_2$ (500) | 76 | 24 |
| $TiO_2$ (600) | 11 | 89 |
| $TiO_2$ (700) | 0 | 100 |

$TiO_2$ P25 consists of mixed phases (83% anatase and 17% rutile), with the anatase fraction decreasing with increasing calcination temperature, as shown in Table 4. There was no difference in phase constitution among the samples thermally treated from 200 to 400 °C.

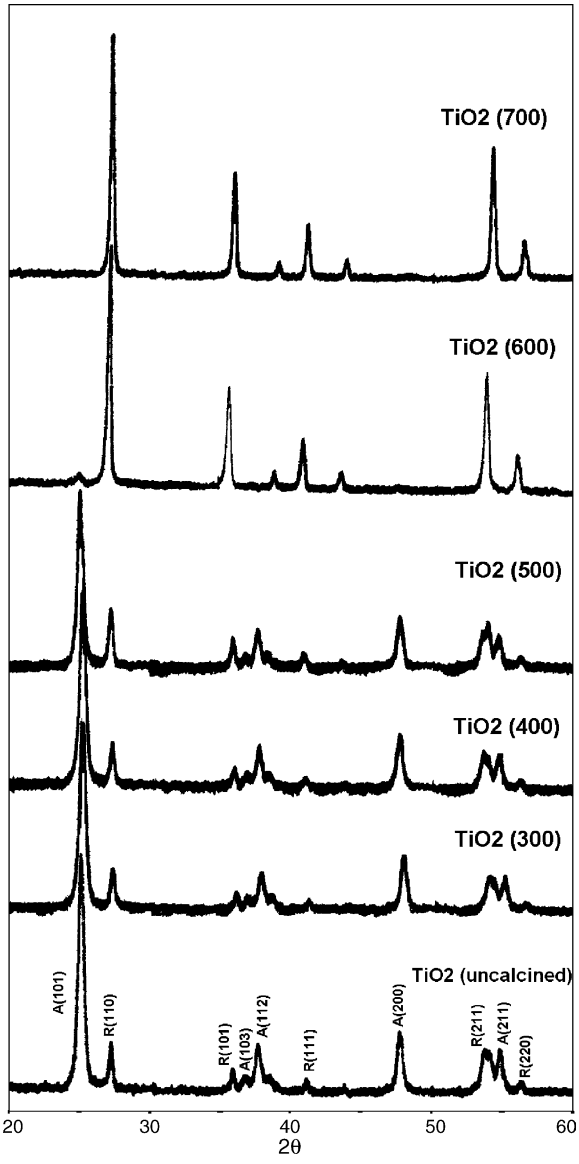


Fig. 2. X-ray diffraction patterns of $TiO_2$ samples.

The anatase–rutile phase transformation took place at 600 °C, and the sample at this temperature had 11% anatase phase and 89% rutile phase. No anatase phase was detected in $TiO_2$ thermally treated at 700 °C. This result was similar to that presented by Kim et al. [18], who reported that the anatase–rutile phase transformation took place at temperatures of 600–800 °C.

The rutile phase content ($X_R$) in crystalline $TiO_2$ was calculated according to the following equation:

$$X_R = \frac{I_R/I_A \cdot K}{1 + I_R/I_A \cdot K} \quad (1)$$

where $I_R$ is the height or area of the peak of the rutile (110) phase in the XRD pattern, $I_A$ that of the anatase (101) phase and $K$ is a constant equal to 0.79 [19].

### 3.2. Photocatalytic degradation

The catalyst photocatalytic activity was evaluated using the photodegradation of phenol as a model pollutant under visible and near-UV irradiation. In this process, both direct and sensitized photocatalysis took place, with the latter predominant, as the glass protection around the lamp retains only part of the UV radiation.

The reduction in phenol concentration was determined by gas chromatography; under the operational conditions used, no other products were observed. According to the literature, the main intermediates can be catechol, hydroquinone and benzoquinone [20–23].

Thus, it is believed that direct photodegradation of phenol to $CO_2$ and $H_2O$ could be occurring, according to step 1 of the ''series–parallel'' mechanism proposed by Salaices et al. [20].

All $TiO_2$ samples showed photocatalytic activity for phenol photodegradation. The highest level of degradation (53%) was obtained with the uncalcined $TiO_2$. Samples calcined between 200 and 500 °C presented similar degradation percentages of nearly 36%.

$TiO_2$ in rutile form is less effective than the anatase form as a photocatalyst for the oxidation of most organic compounds. Therefore, it is normal that the $TiO_2$ calcined at 600 and 700 °C showed lower photoactivity than that thermally treated at 500 °C [5]: $TiO_2$ (600) achieved 18% phenol degradation, while $TiO_2$ (700) reached only 13%.

The better result for uncalcined $TiO_2$ may be explained by its anatase phase structure and hydroxyl groups on the powder surface. It has been found that these two aspects can enhance photocatalytic reactions [19]. An increase in rutile content results in a decrease in surface adsorbed water and hydroxyl groups, which are crucial for photocatalysis, since they react with photoexcited holes on the catalyst surface and produce hydroxyl radicals, which in turn are powerful oxidants in degrading organics in water [17,24].

The amount of chemisorbed water directly bound to Ti(IV) ions on the surface is higher at lower temperature. As the calcination temperature of $TiO_2$ increases, the density of surface-bound hydroxyl groups ($OH^-$) or chemisorbed $H_2O$ decreases, subsequently reducing the probability of $OH^-$ production and thus retarding the photoreaction. The greater the number of surface $OH^-$ groups, the faster is the photocatalytic reaction [25].

These surface-adsorbed water and hydroxyl groups are also related to the $TiO_2$ $pH_{(ZPC)}$ value that varies with thermal treatment, since the $TiO_2$ samples calcined at higher temperatures undergo only partial rehydroxylation when exposed to water. Thus, the higher activity of uncalcined $TiO_2$ must also be due to its low $pH_{(ZPC)}$ value, which facilitated phenol degradation.

Photocatalytic phenol degradation using uncalcined $TiO_2$ can be described by a Langmuir–Hinshelwood model of pseudo-first order $[\ln(C_0/C) = k_{ap}t]$ with an apparent reaction rate constant of 0.1459 $h^{-1}$ and a correlation coefficient of 0.9921.

Fig. 3 shows the change in phenol concentration with photoirradiation time. The concentration decreased with time in the seven systems, but uncalcined $TiO_2$ showed the best photocatalytic performance, in spite of the surface area and fraction of the crystalline phases being equal to those of $TiO_2$ calcined above 500 °C.

These results differ from the traditional idea that a large specific surface area is favorable for the reaction, because this large area may dilute the concentration of active sites for phenol adsorption, and that an increase in catalyst crystal size is detrimental to catalytic activity, since it results in a reduction of the contact area between reactant and catalyst.

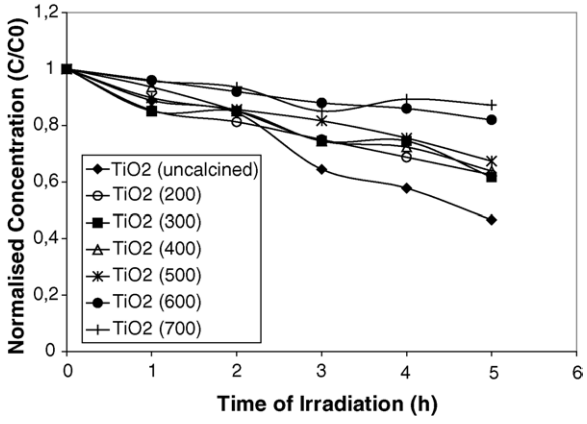


Fig. 3. Profiles of the phenol degradation.

Thermal treatment led to changes in the crystallinity, surface area, and size of $TiO_2$ particles. All these factors may affect the photocatalytic activity, but it is difficult to estimate the separate contribution of each of them [26,27].

When all the anatase is transformed into rutile, the sample still has a certain activity. This indicates that both anatase and rutile contribute to the reaction, but the anatase phase is more active than rutile. However, it is difficult to relate crystallite phases and activity. As shown above, the activity is also related to the textural properties.

Although the uncalcined $TiO_2$ and $TiO_2$ calcined from 200 to 500 °C showed the same surface area, uncalcined $TiO_2$ led to the highest level of phenol degradation, indicating that the thermal treatment influenced the other textural properties and the photocatalytic activity.

This result is indicative that phenol degradation in this case may occur by direct photocatalysis, in which the absorption of energy greater than the $TiO_2$ bandgap energy (UV irradiation) promotes the injection of a valence band electron into the conduction band, causing charge separation. Oxidative degradation is attributed to indirect reaction at positive holes, where adsorbed water or a hydroxyl group is oxidized to a hydroxyl radical ($OH^\bullet$), which then reacts with phenol. The ratio between the catalyst surface area and the initial phenol concentration is an important factor affecting the ability of phenol to undergo sensitized photocatalysis. This results from the necessity for direct interaction between a short-lived excited state of phenol and a $TiO_2$ particle to achieve charge injection into the conduction band [28].

## 4. Conclusions

The results presented in this work showed that the temperature of calcination strongly influenced the structure and photocatalytic activity of $TiO_2$.

In terms of textural analysis, an increase in calcination temperature caused a reduction in the specific surface area after thermal treatment above 500 °C. The external surface area and mean pore diameter decreased with increasing temperature.

It was verified that photocatalysts present acidic sites that are responsible for propene formation in isopropanol decomposition and that with thermal treatment there was an increase in the specific acidity, leading to an increase in acidic force and a slight increase in basicity related to the ratio between acetone and propene formation.

The XRD patterns for $TiO_2$ showed that this was constituted of anatase and rutile phases. The percentage of the latter increased as the calcination temperature increased and the anatase–rutile phase transformation occurred at 600 °C.

As the luminous source emitted visible and near-UV radiation, direct and sensitized photocatalysis could occur in this process. The greatest activity for phenol degradation was obtained with the uncalcined $TiO_2$, in spite of the similarity in the values for surface area and crystalline phase fraction in relation to the other catalysts. This can be explained by the presence of surface-adsorbed water and hydroxyl groups on the uncalcined $TiO_2$ surface. This is an indication that thermal treatment had a greater influence on the activity than on the textural properties.

## Acknowledgements

The authors thank CAPES (Coordenação de Aperfeiçoamento de Pessoal de Nível Superior) for its financial support, DEQ/UFSCAR for XRD measurements and DEGUSSA for $TiO_2$ samples.

## References

[1] J.B. De Heredia, J. Torregrosa, J.R. Domínguez, J.A. Peres, J. Hazard. Mater. B83 (2001) 255.
[2] A.M. Peiró, J.A. Ayllón, J. Peral, X. Doménech, Appl. Catal. B: Environ. 30 (2001) 359.
[3] S. Espulgas, J. Giménez, S. Contreras, E. Pascual, M. Rodríguez, Water Res. 36 (2002) 1034.
[4] L. Gao, Q. Zhang, Scr. Mater. 44 (2001) 1195.
[5] J.C. Yu, J. Lin, D. Lo, S.K. Lann, Langmuir 16 (2000) 7304.
[6] K.-H. Wang, H.-H. Tsai, Y.-H. Hsieh, Appl. Catal. B: Environ. 17 (1998) 313.
[7] R. Van Grieken, J. Aguado, M.J. López-Muñoz, J. Marugán, J. Photochem. Photobiol. A: Chem. 3010 (2002) 1.
[8] M. Kang, Appl. Catal. B: Environ. 37 (2002) 187.
[9] L. Saadoun, J.A. Ayllón, J. Jiménez-Becerril, J. Peral, X. Doménech, R. Rodríguez-Clemente, Appl. Catal. B: Environ. 21 (1999) 269.
[10] F.J. Maldonado-Hódar, C. Moreno-Castilla, J. Rivera-Utrilla, Appl. Catal. A: Gen. 203 (2000) 151.
[11] H. Liu, H.T. Ma, X.Z. Li, W.Z. Li, M. Wu, X.H. Bao, Chemosphere 50 (2003) 39.
[12] S.J. Gregg, K.S.W. Sing, Adsorption, Surface Area and Porosity, Cap. 2 e 4, second ed., Academic Press, Inc., London, 1982.
[13] J. Horniakova, M. Králik, A. Kaszonyi, D. Mravec, Micropor. Mesopor. Mater. 46 (2001) 287.
[14] A.J. Patil, M.H. Shinde, H.S. Potdar, S.B. Deshpande, S.R. Sainkar, S. Mayadevi, S.K. Date, Mater. Chem. Phys. 68 (2001) 7.
[15] A. Gervasini, A. Auroux, J. Catal. 131 (1991) 190.
[16] D. Das, H.K. Mishra, K.M. Parida, A.K. Dalai, J. Mol. Catal. A: Chem. 189 (2002) 271.
[17] E. Pelizzetti, C. Minero, Electrochim. Acta 39 (1993) 47.
[18] D.J. Kim, S.H. Hahn, S.H. Oh, E.J. Kim, Mater. Lett. 57 (2002) 355.
[19] J. Yang, D. Li, X. Wang, X. Yang, L. Lu, Mater. Sci. Eng. A328 (2002) 108.
[20] M. Salaices, B. Serrano, H.I. de Lasa, Chem. Eng. Sci. 59 (2004) 3.
[21] J. Chen, L. Eberlein, C.H. Langford, J. Photochem. Photobiol. A: Chem. 148 (2002) 183.
[22] J. Araña, E.T. Rendón, J.M.D. Rodríguez, J.A.H. Melián, O.G. Díaz, J.P. Peña, Appl. Catal. B: Environ. 30 (2001) 1.
[23] H. Chun, W. Yizhong, T. Hongxiano, Chemosphere 41 (2000) 1205.
[24] Z. Ding, G.Q. Lu, P.F. Greenfield, J. Phys. Chem. B 104 (2000) 4815.
[25] M.R. Dhananjeyan, V. Kandavelu, R. Renganathan, J. Mol. Catal. A: Chem. 151 (2000) 217.
[26] T. Ohno, K. Tokieda, S. Higashida, M. Matsumura, Appl. Catal. A: Chem. 244 (2003) 383.
[27] Y. Tanaka, M. Suganuma, J. Sol–Gel Sci. Technol. 22 (2001) 83.
[28] M.S. Dieckmann, K.A. Gray, Water Res. 30 (5) (1996) 1169.